Published online 10 June 2016

Nucleic Acids Research, 2016, Vol. 44, No. 17 ***8417–8424***
doi: 10.1093/nar/gkw526

Crystal structure of a poly(rA) staggered zipper at acidic pH: evidence that adenine N1 protonation mediates parallel double helix formation

Michael L. Gleghorn[1,3], Jianbo Zhao[2,3], Douglas H. Turner[2,3] and Lynne E. Maquat[1,3,*]

[1]Department of Biochemistry and Biophysics, School of Medicine and Dentistry, University of Rochester, Rochester, NY 14642, USA, [2]Department of Chemistry, University of Rochester, Rochester, NY 14627, USA and [3]Center for RNA Biology, University of Rochester, Rochester, NY 14642, USA

Received February 02, 2016; Revised May 31, 2016; Accepted June 01, 2016

ABSTRACT

We have solved at 1.07 Å resolution the X-ray crystal structure of a polyriboadenylic acid (poly(rA)) parallel and continuous double helix. Fifty-nine years ago, double helices of poly(rA) were first proposed to form at acidic pH. Here, we show that 7-mer oligo(rA), i.e. rA_7, hybridizes and overlaps in all registers at pH 3.5 to form stacked double helices that span the crystal. Under these conditions, rA_7 forms well-ordered crystals, whereas rA_6 forms fragile crystalline-like structures, and rA_5, rA_8 and rA_{11} fail to crystallize. Our findings support studies from ∼50 years ago: one showed using spectroscopic methods that duplex formation at pH 4.5 largely starts with rA_7 and begins to plateau with rA_8; another proposed a so-called 'staggered zipper' model in which oligo(rA) strands overlap in multiple registers to extend the helical duplex. While never shown, protonation of adenines at position N1 has been hypothesized to be critical for helix formation. Bond angles in our structure suggest that N1 is protonated on the adenines of every other rAMP–rAMP helix base pair. Our data offer new insights into poly(rA) duplex formation that may be useful in developing a pH sensor.

INTRODUCTION

In recent years, synthetic nucleic acids have been utilized as materials to generate nanostructures for a variety of applications, including targeted delivery of gene silencing molecules (i.e. siRNA) (1). The programmable and self-assembling features of nucleic acids through base pairing and other interactions make them ideal substrates to produce nanomaterials for biomedical and other applications—a burgeoning field. However, such applications require understanding the biophysical properties of nucleic acids beyond simple base pairing. For example, G-quadruplexes possess particular structural capabilities that allow them to be engineered as scaffolds to deliver anti-cancer drugs or serve as targets for anti-HIV therapies, since evidence indicates that HIV contains G-quadruplexes (2,3).

In 1957, Fresco and Doty reported the discovery that poly(rA) of $\geq rA_{29}$ forms fibers at acidic pH that were speculated to be double helices (4). These fibers were later called 'interrupted helices' because their composite poly(rA) strands were thought to overlap in different registers (5). The interrupted helix could be formed, dissociated and then re-formed by sequentially altering the pH (5). Applequist and Damle proposed in 1965 that the most energetically favorable structure formed by oligo(rA) is a 'staggered zipper', in which oligo(rA) strands overlap in all registers with no more than a single nucleotide gap (6). Thermodynamic studies found that duplex formation in acidic conditions requires a minimum length of rA_6 or rA_7 (7).

In 1961, Rich *et al.* proposed that a parallel double helix of poly(rA) forms in acidic conditions in a way that differs from Watson–Crick base pairing (8). It was proposed that the Hoogsteen edges of two adenosines on opposite strands of the helix interact symmetrically so that the N6 of each adenosine hydrogen bonds with N7 of the reciprocal adenosine. At the same time, the Watson-Crick edges of the two adenosines interact with the phosphate group of the reciprocal adenosine. Protonation at each N1 was proposed to contribute a helix stabilizing and neutralizing interaction with the non-bridging oxygen of the phosphodiester backbone of its paired partner. This A–A arrangement differs from traditional Watson-Crick base pairs by an additional involvement of the phosphate backbone from each rAMP in what are actually 'rAMP–rAMP pairs'. Nonetheless, we will refer to these rAMP–rAMP pairs as rA–rA 'base pairs'. A recent X-ray crystal structure of a parallel but discontinuous double helix formed using rA_{11} at pH 7 (9) is consistent with the acidic pH model of Rich et al. (8) except that it contains ammonium ions (NH_4^+), which were not part of the Rich model. The ammonium ions are positioned be-

*To whom correspondence should be addressed. Tel: +1 585 273 5640; Fax: +1 585 275 6007; Email: lynne_maquat@urmc.rochester.edu

tween each unprotonated N1, substituting for the lack of protonated N1, and the most proximal non-bridging oxygen of the phosphate group of the rA to which it base pairs (9). UV thermal denaturation experiments using oligo(rA) lengths ranging from rA_{10} to rA_{16} showed that the presence of ammonium ions could functionally replace acidic conditions as low as pH 4, thus allowing duplexes to form at more neutral pH (9).

The propensity for adenine to be protonated as acidity increases is thought to occur in the following order: N1 > N7 > N3 (10,11). Studies indicate that the probability of protonation of adenine in the context of adenosine, i.e. adenine with a ribose sugar, is 96.1% for N1, 3.2% for N7 and 0.3% for N3 (11,12). While the pK_a of adenosine N1 is ∼3.63, the exact pK_a values for adenosine N7 and N3 are difficult to ascertain: both may be protonated, or either may be the sole site of protonation due to repulsion effects (11). Nevertheless, it has alternatively been reported for adenosine that gas-phase protonation preferentially occurs at N3 over N1 (13), and that N7 has the lowest proton affinity (14). Notably, whereas deoxy-adenosine behaves more like adenine since both are slightly preferentially protonated at N1 relative to N3 (15,16), cyclic AMP is almost equally protonated at N1 and N3 (12).

Here, we show the first structure at low pH of a poly(rA) parallel duplex. The structure is composed of rA_7 and was solved at 1.07 Å resolution (Table 1) and pH 3.5. Among our new findings, rA_7 assembles to form a zipper that is staggered (i.e. oligo(rA) is in different registers when comparing one strand of the double helix to the opposite strand of the double helix) and interrupted (i.e. there is discontinuity in the backbone of each strand) to form a perfectly straight double helix that spans the entire length of the crystal. The parallel helix has inherent symmetry that is entwined with crystallographic symmetry. This results in a repeating rA_2 structure that, when projected through its crystallographic space group symmetry, generates a complete helix as well as crystal lattice. In our crystal structure, each base pair alternates between having the N1 position of adenine protonated and the N1 position of adenine unprotonated but coordinated to a phosphate-bridging ammonium ion.

MATERIALS AND METHODS

To generate crystals, rA_7 (idtdna.com, the source of all oligo(rA) used here) was dissolved in water to 10 mM, and then diluted 1:10 (v/v) in 0.75% polyethylene glycol 1000. One microliter of this dilution was mixed with 1 μl of reservoir solution (0.24 M ammonium sulfate and 0.06 M citric acid pH 3.5.) to generate a hanging-drop, which was subjected to vapor-diffusion over a 1 ml reservoir solution. Crystals appeared within one day of incubation at 20°C. While ammonium sulfate and/or citric acid concentrations could be slightly varied, both were required to produce crystals, and the concentrations used in this study produced the largest crystals.

Crystals were moved to a 50/50 (v/v) paratone-N/silicon oil solution and flash frozen in liquid nitrogen. X-ray diffraction data were collected remotely at the Stanford Synchrotron Radiation Lightsource (SSRL). Data were scaled (17,18) in different space groups, and molecular replacement was performed using Phaser (19) in Phenix (20). A 2-mer oligo(rA) section from one strand of the Safaee *et al.* rA_{11} structure (9) was initially used in molecular replacement experiments to identify starting phases. Our best solution was obtained in the $P4_22_12$ space group where the asymmetric unit is rA_2. Model building was performed using WinCoot (21), and refinements were performed using Phenix (20) and CCP4 (22).

Quantum mechanics was used to predict bond angles for adenosine and 9-methyladenine as neutral molecules and with N1, N3, or both N1 and N3 protonated. Calculations were carried out at the 6–311++G** level using Hartree-Fock, B3LYP (23,24), and MP2 methods using Gaussian 09 [http://www.gaussian.com/]. All minimizations were followed by frequency calculations to confirm the global minimum.

Table 1. X-ray crystallographic statistics of the rA_7-generated crystal structure[a]

Data Collection Statistics (PDB 5K8H)	
Space group	$P4_22_12$
a, *b*, *c* [Å]	21.25, 21.25, 14.95
Resolution [Å]	21.25–1.07 (1.14–1.07)
R_{merge}	0.127 (1.059)
R_{pim}	0.032 (0.333)
$I/\sigma I$	15.0 (3.1)
CC 1/2	0.994 (0.987)
Completeness [%]	97.6 (87.2)
Multiplicity	19.3 (8.9)
Refinement statistics	
Resolution [Å]	15.03–1.07
No. of reflections	1663
R_{work}/R_{free}[b]	0.105/0.106
Average *B*-factors (Å^2)	
rA (non-hydrogen)	18.51
Waters	47.39
Single ammonium ion	18.54

[a]Values in parentheses represent the highest resolution shell.
[b]R_{free} is comprised of 9.14% of the total reflections.

RESULTS AND DISCUSSION

rA_7 self-assembles into a parallel double helix

Solving the structure of rA_7 crystals revealed that the asymmetric unit is optimally defined as a single rA_2 strand. Applying crystallographic symmetry revealed a crystal lattice made up of bundled poly(rA) parallel duplex strands where, unlike double-stranded (ds)DNA or dsRNA antiparallel duplexes, both strands have the same 5′-3′ polarity (Figure 1A-B). The poly(rA) parallel double helices alternate in 5′-3′ directionality within the crystal lattice (Figure 1C), manifesting a right-handed helical turn that repeats every eight base pairs (Figure 1B and D). Viewing a cross-section of the crystal lattice like a tic-tac-toe board, helices in the middle square and four-corner squares are oriented with the same 5′-3′ directionality, whereas the remaining four squares are oriented in the opposite direction (Figure 1C). In other words, when the tic-tac-toe board is rotated diagonally to reveal a diamond-shape, helices in the same horizontal row manifest the same directionality, which is opposite to the directionality of adjacent horizontal rows (Figure 1C). Notably, the crystal lattice comprised of rA_{11} poly(rA)

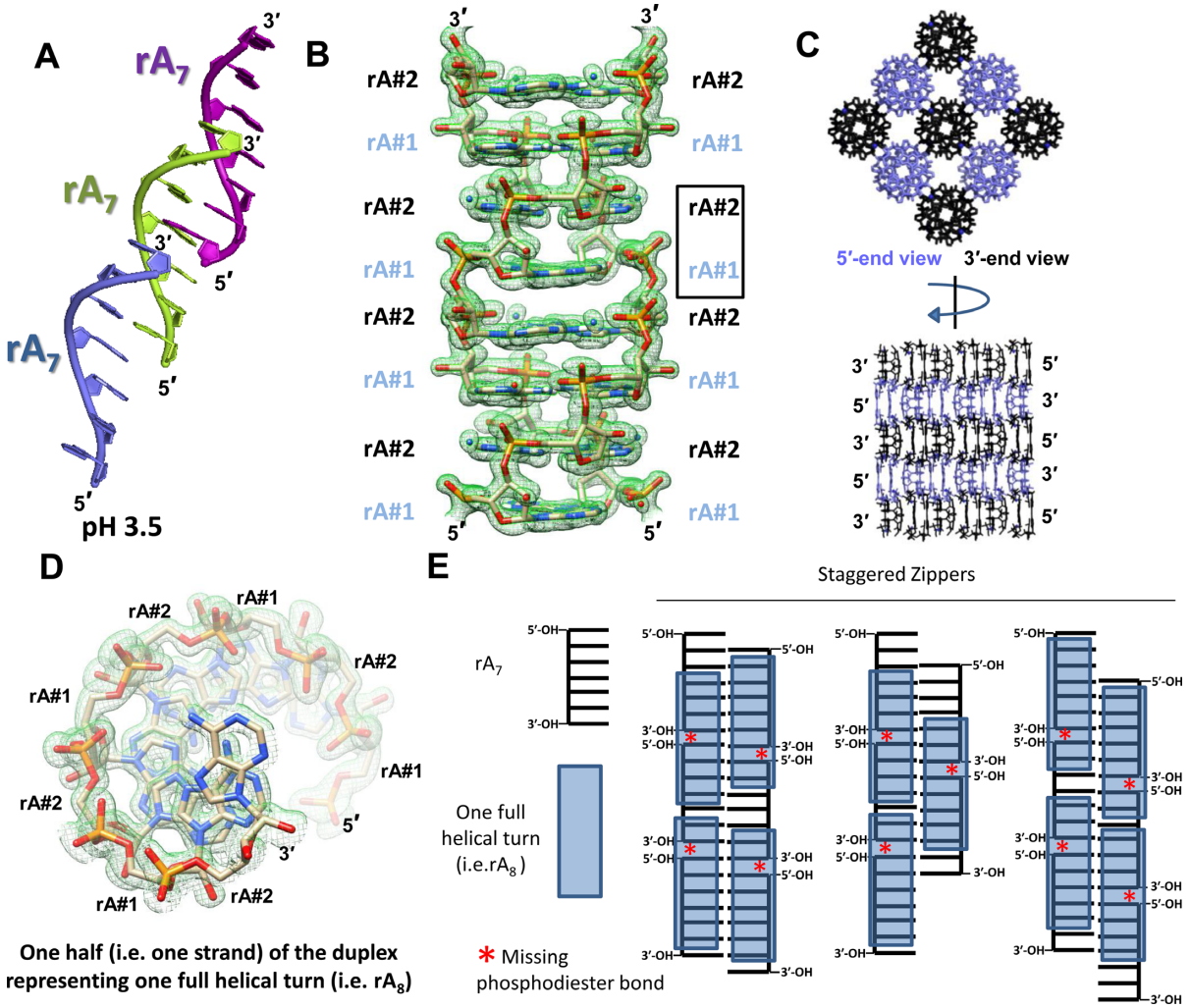

Figure 1. X-ray crystal structure of the rA_7 staggered-zipper parallel and continuous double helix. (**A**) At pH 3.5, rA_7 strands self-assemble to form a parallel poly(rA) duplex. (**B**) The rA_7 strands form staggered zipper helices that average over the crystal to yield electron density indicative of a continuous parallel helix. Shown is a σ_A-2Fo-Fc electron density map at 1.2σ intensity that is limited to a 1.7 Å radius of atoms. The asymmetric (i.e. repeating) unit of the crystal is comprised of a single rA_2 strand that, via crystallographic symmetry, forms strands that constitute an elongated helix with 8 rA pairs per full turn of the helix. (**C**, Top) A cross-section of the rA_7 crystal lattice illustrating that each helix appears as a 'donut' shape. The cross-section is limited to a square 'tic-tac-toe' board that has been rotated 45° so that blue- and black-colored helices have opposite polarities and that helices on the same horizontal of the board have the same polarities. (C, Bottom) A side-view of (C, Top) illustrates the alternating layers of helices having opposite polarities. (**D**) A σ_A-weighted $2F_o - F_c$ electron density map as in B, but for rA_8 atoms that constitute one full turn of the helix, illustrating the repeating rA_2 asymmetric unit and the continuation of the phosphate backbone across the full-length of the crystal lattice via 5'- and 3'-end joining of rA_7 molecules. (**E**) Illustration of how rA_7 molecules form a crystal structure of staggered zipper helices, i.e. form a helical duplex of staggered rA_7 molecules. In the crystal, each full turn of the helix (i.e. 8 rAs per strand; blue boxes) is missing at least one and maximally two phosphate group(s) (red asterisks). However, since the asymmetric unit of the crystal is rA_2, and each rA_7 strand contributes only six phosphates, the averaged phosphate occupancy is 6/7 or 0.86.

duplexes at neutral pH shares a similar alternating pattern of helix orientation (9).

Each rA_2 in our structure pairs with another rA_2 that is generated by helical and crystal symmetry (Figure 1B). If we defined each rA in a rA_2 asymmetric unit as rA#1 and rA#2, then rA#1 pairs with symmetry-generated rA#1, and rA#2 pairs with symmetry-generated rA#2. While the helix is composed of rA_7 molecules (Figure 1A), electron density for the phosphate backbone in the structure is continuous not only within the asymmetric unit but also from one asymmetric unit to the next, thereby forming an apparently unending RNA strand and helix (Figure 1B–D). Since the termini of rA_7 consist of 5'- and 3'-OH groups, a phosphate group is missing between adjacent rA_7 molecules that constitute the same strand of an extended double helix (Figure 1E). Thus, the crystal structure represents an average of many different registers of rA_7 strand alignments. Assuming that there is no preferential register, the gaps between each strand must be missing phosphate electron density once in every stretch of seven rAs, indicating that the occupancy of phosphate is 0.86.

To determine the preferred occupancy of the phosphate backbone, we permitted Phenix software to refine phosphate occupancy and B-factor values. Given that there is no rA_7 5′ phosphate, and the oxygen of each rA_7 5′ OH may adopt a conformation that differs from the conformation

of an oxygen within a phosphodiester bond, we additionally permitted the occupancy of each rA_7 5′ oxygen to be refined. We did not permit 3′ oxygens to be refined since electron density maps failed to indicate an overestimation of 3′ oxygen occupancy. On average, the occupancies of refined phosphate and oxygen atoms revealed that phosphate occupancies are 0.94 for rA#1 (where the 5′ oxygen and one non-bridging oxygen refined to an occupancy of 1.0) and 0.915 for rA#2. Any positive deviations from the predicted phosphate occupancy of 0.86 could be attributed to potential water molecules bound at the gaps between rA_7 molecules so as to contribute additional electron density at these positions.

Crystallization at pH 3.5 is specific to rA_7. While crystals form with rA_6, the crystals were fragile to touch, failed to configure the well-ordered rigid morphology obtained with rA_7 (Supplementary Figure S1), and could not be captured to collect diffraction data. No crystals were observed with rA_5, rA_8 or rA_{11} under our conditions or when the concentrations of ammonium sulfate and/or citric acid were varied at pH 3.5 (data not shown).

Comparison of acidic rA_7-generated and neutral pH rA_{11}-generated helices

The asymmetric unit of the Safaee *et al.* rA_{11} pH 7 structure (9) is composed of 10 rA−rA interactions (i.e. a 10-base pair duplex) and a rA overhang on both strands. Each rA overhang pairs with the rA overhang of another asymmetric unit to form a continuous 'quasi-continual' duplex. Duplex units tilt at each asymmetric unit juncture, and there is no continuation of phosphate backbone electron density at each junction on either strand. In our structure, the 'donut hole', i.e. the 'tube' that spans the length of the crystal lattice (Figure 1C), is continuously empty; in contrast, the rA_{11} pH 7 structure is blocked at asymmetric unit junctures because of their tilt and imperfect helices.

To compare the rA_7 and rA_{11} crystal structures, we first generated a 2-base pair duplex from the rA_2 asymmetric unit of the rA_7 structure by adding the paired rA_2 symmetry mate (i.e. the symmetry mate that is rotated 180° around the central axis of the helix). Using ARTS (25), the best alignment of the rA_{11} structure to our 2-base pair duplex is residues A7–A8:B6–B7 (i.e. using our nomenclature, rA#7-rA#8 of strand A paired to rA#6 and rA#7 in strand B), which has a RMSD of 0.19 Å. This rA_{11} structure 2-base pair duplex resides near the middle of its 10-base pair duplex.

We next used 3DNA (v2.3-2016feb12, specifically 'simple' parameters described as 'intuitive for non-Watson–Crick base pairs';26,27) to compare the helical and individual nucleotide structural parameters of the rA_7 2-base pair duplex and the rA_{11} 10-base pair duplex. Many of the helical and base pair parameter values of the two helices are grossly similar (Table 2). For example, our rAs are in the *anti* conformation since the glycosidic angle for rA#1 is 183.5° and for rA#2 is 186°, similar to the 187° average glycosidic angle for the Safaee et al. structure (9). Additionally, maximum torsion angles for 3' endo sugar puckers are 37.4° and 38.5° for, respectively, rA#1 and rA#2 in our structure, compared to a somewhat similar average of 43.5° for the rAs of the rA_{11} structure (9). Pseudorotational phase angles are slightly different for rA#1 and rA#2 at 16.4° and 11.8°, respectively, which are distinct from the 10.7° average angle for the rA_{11} structure (9).

There are some notable differences between the two structures reflected in 3DNA base pairing parameters and the helix itself (Table 2). Most notably, the rA_7 structure has buckle values of −3.62° and −4.46° for, respectively, rA#1–rA#1 and rA#2–rA#2, which are less than the average buckle value of −8.26° for all 10 base pairs in the rA_{11} structure. Additionally, while rA_7 shift, slide, stagger, tilt and roll values are zero and the opening value is 180°, the respective rA_{11} values are close to but not precisely comparable (Table 2). The precise values for rA_7 highlight the entwinement of helical symmetry with crystal symmetry (see below), reflecting the ability to generate helices within a crystal sufficiently uniform to be described by a rA_2 asymmetric unit.

The model of Rich *et al.* placed adenines at a tilt, today called a 'propeller' angle, of 10–11° relative to the axis of the helix (8). In our structure, the propeller angle is 10.68° for rA#1–rA#1, which is protonated at N1, and 11.67° for rA#2–rA#2, which is unprotonated and coordinated with ammonium at N1 (see below) as are all base pairs in the Safaee et al. structure. Base pairs 5 through 9 of the Safaee et al. structure also have propeller angles that approximate 11°, whereas base pair 4 has a 8.04° angle, base pair 3 has a 5.23° angle, and base pairs 1, 2 and 10 have the most acute propeller angles that range from −4.06° to 4.34° (Table 2). The similar propeller angles between our structure and a continual 5-base pair region of the Safaee et al. structure, which can be extended to 7-base pairs if slightly more acute propeller angles are allowed, might explain why rA_7 is the shortest unit capable of generating stable helices; the similar propeller angles may also explain why we find that $rA_{>7}$ fails to form perfectly straight and continuous poly(rA) helices. For the Safaee et al. structure, we suggest that the 7-base pairs that have propeller angles most similar to those in our structure – in particular the middle of the 7-base pairs that align best to our structure – is the nucleus for helix formation and that the rest of the 10-base pair unit fails to maintain consistent helix parameter values. We also suggest that the break after each rA_7 in our structure provides relief for helical restraints so that each subsequently annealed rA_7 can form the helix without paying a restraint penalty as the helix lengthens.

Evidence that adenines in every other base pair of the helix are protonated at N1

Resolution below 1 Å is usually required to visualize hydrogen atoms (28) and even then only a partial description of all hydrogens has been achievable, depending on *B*-factor values (29). Nevertheless, we can infer the protonation states of adenine by measuring its bond angles (9), which in our structure are especially reliable given that the coordinate error estimation performed by Phenix is 0.06 Å.

The best R_{free} values were obtained when we positioned the hydrogens of adenines as would be expected at neutral pH (i.e. one hydrogen on C2, one hydrogen on C8, and two hydrogens on N6) and, rather than forcing a neutral pH configuration, incrementally weakened geometric restraints

Table 2. Comparative 3DNA analyses of our rA_7 structure and the rA_{11} structure of Safaee *et al.* (9)[a]

	3DNA Base Pair Parameter Values (Å)						3DNA Base Pair Parameter Values (°)					
	Shift	Slide	Rise	Shear	Stretch	Stagger	Tilt	Roll	Twist	Buckle	Propeller	Opening
rA7, pH 3.5 structure	Step from previous pair						Step from previous pair					
rAMP#1–rAMP#1 (N1 protonated)	0	0	3.72	-7.85	0.51	0	0	0	41.21	-3.62	10.68	180
rAMP#2–rAMP#2 (N1 neutral and ammonium coordinated)	0	0	3.75	-7.87	0.38	0	0	0	48.79	-4.46	11.67	180
rA11, pH 7 structure (PDB 4JRD)												
rAMP#1 (A) overhang												
rAMP#2 (A)–rAMP#1 (B)	Step from previous pair			-7.96	0.41	-0.03	Step from previous pair			-13.64	-4.06	-179.47
rAMP#3 (A)–rAMP#2 (B)	0.67	-1.62	3.49	-7.86	0.38	-0.33	2.57	6.09	32.66	-10.20	-3.53	-179.33
rAMP#4 (A)–rAMP#3 (B)	-0.41	-0.21	3.82	-7.96	0.43	0.02	-3.27	-1.57	42.53	-10.15	5.23	179.91
rAMP#5 (A)–rAMP#4 (B)	-0.31	0.30	3.75	-7.95	0.50	0.1	0.30	-1.52	41.21	-9.24	8.04	179.15
rAMP#6 (A)–rAMP#5 (B)	0.35	0.47	3.78	-7.95	0.46	0.08	-0.76	-1.56	43.72	-7.36	10.12	-179.98
rAMP#7 (A)–rAMP#6 (B)	0.4	-0.31	3.76	-7.97	0.60	0.06	-0.26	0.09	41.38	-5.15	12.87	-176.77
rAMP#8 (A)–rAMP#7 (B)	-0.17	0.01	3.81	-7.88	0.66	-0.02	0.68	1.12	44.20	-7.82	11.89	-179.56
rAMP#9 (A)–rAMP#8 (B)	-0.11	0.19	3.83	-7.91	0.56	-0.05	-0.06	-0.50	41.53	-7.03	13.68	179.23
rAMP#10 (A)–rAMP#9 (B)	-0.06	-0.42	3.78	-7.94	0.47	-0.03	-0.73	-0.07	41.85	-3.78	13.76	-179.24
rAMP#11 (A)–rAMP#10 (B)	-0.11	-0.09	3.56	-7.92	0.42	0.1	-0.34	-1.40	39.81	-3.03	4.34	-178.91
rAMP#11 (B) overhang												

[a]Blue and green denote differences between rA_7 crystal rA#1 and rA#2. Dark purple indicates propeller angles that are ~11°, and faded purple shows progressively smaller propeller angles.

to allow the adenine rings to fit the electron density data. That is, we assumed no protonation, but relied on the high-resolution electron density data to report bond angles able to reveal protonation.

To develop bond angle standards representative of different adenine protonation states for comparison to our structure, we first updated a survey that correlated bond angles to adenine protonation states (30). To do this, we identified 467 small molecule structures in the Cambridge Structural Database (CSD) that include 'adenine'. Within these adenine-containing molecules we found 262 adenines that are neutral, 65 that are protonated at N1, twelve that are protonated at N3, and none that are protonated at N1 and N3 (Supplementary Tables S1–S3; Table 3).

A second set of standards was created using quantum mechanics to predict bond angles for adenosine with N1, N3 or both N1 and N3 protonated and when the ribose of adenosine was replaced by a methyl group (Supplementary Table S4; Table 3). Very similar results were obtained for adenosine and 9-methyladenine and with three different levels of theory (Supplementary Table S4).

C2–N1–C6 bond angles for the first paired rAs (i.e. rA#1–rA#1) in our structure are ~126.8° (Figure 2A and B; Table 4). Comparing these bond angles to bond angles derived from small-molecule crystal structures in the CSD (Table 3) or bond angles predicted using quantum mechanics (Table 3) indicated that every other adenine in our structure (Figure 1B) is protonated. Based on structures in the CSD, the C2–N1–C6 angle is 118.6° ± 1.1° when N1 is neutral and 124.0° ± 2.5° when N1 is protonated (Table 3). Similarly, our quantum calculations predicted C2-N1-C6 bond angles of 118.6° when N1 is neutral and 123.4° when N1 is protonated (Table 3; Supplementary Table S4). By either calculation, N1 protonation values more closely approximate the 126.8° C2–N1–C6 bond angle for each rA#1 in rA#1–rA#1. The intermittent alternating paired rA#2s, i.e. those that reside between the N1 protonated pairs, have C2-N1-C6 bond angles on average of ~120.2° (Figure 2E and F; Table 4), which is closer to the measured and predicted bond angle when N1 is neutral (Table 3).

Table 3. Bond angles associated with different protonation states of adenine

Angle	CSD Derived Values (°)		
	Neutral*	N1 protonated**	N3 protonated***
C2-N1-C6	118.6 ± 1.1	124.0 ± 2.5	119.3 ± 0.8
C2-N3-C4	110.7 ± 1.2	111.7 ± 0.9	117.3 ± 0.6

Quantum Chemistry Derived (B3LYP) Values (°) for Adenosine				
	Neutral	N1 protonated	N3 protonated	N1 & N3 protonated
C2-N1-C6	118.6	123.4	120.1	124.3
C2-N3-C4	111.6	113.8	116.9	117.8

*262 adenines, **65 adenines, ***12 adenines

Table 4. Adenine bond angles of the rA_7 structure.[a]

Angle	rA#1	rA#2
C2-N1-C6 angle (°)	126.8	120.2
C2-N3-C4 angle (°)	112.0	112.1

[a]Modeled with neutral hydrogen positions

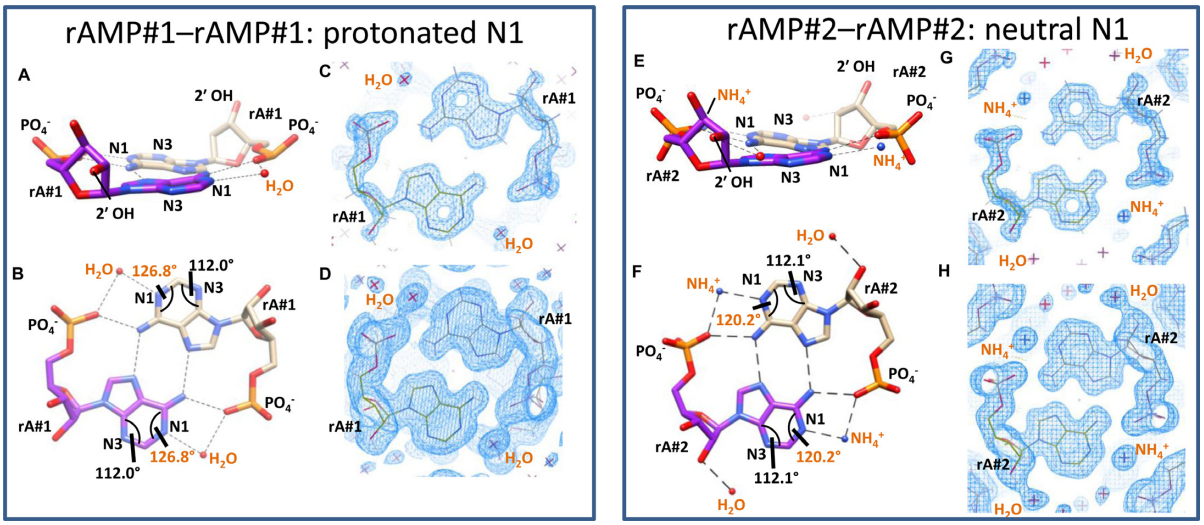

Figure 2. A comparison of alternating odd (rA#1–rA#1) and even (rA#2–rA#2) rA–rA pairs. (**A**–**D**) A single rA#1–rA#1 pair is illustrated. Panels E, F, G and H correspond, respectively, to panels A, B, C and D, and orange labels specify differences. (A) A side view illustrating the ∼11° propeller tilt of each rA as predicted by Rich *et al.* (8). This tilt facilitates the interaction between the N6 of one rA#1 and non-bridging phosphate oxygen of its paired rA#1. Atoms and molecules are labelled. (B) As in A, but rotated 90° to illustrate that C2–N1–C6 angles are sufficiently large to indicate that N1 is protonated. Also shown are the modelled water molecules that exist between the protonated N1 and non-bridging phosphate oxygen. (C) Illustration of a σ_A-weighted $2F_o - F_c$ electron density map at 0.9969e/Å^3 intensity. (D) As in C, but at 0.1623e/Å^3 intensity. Note that at lower σ, electron density for the N1-coordinated water molecule appears to merge with electron density of the paired phosphate. (**E**–**H**) A single rA#2–rA#2 pair is illustrated.

The C2–N3–C4 bond angles in our structure are also consistent with an N1 protonated rA#1 and neutral rA#2 (Tables 3 and 4). Notably, the C2–N3–C4 angles of 112° for rA#1 and rA#2 (Table 4) rule out N3 protonation, which is expected to have a C2–N3–C4 angle of 117° (Table 3).

Within individual strands, electron density profiles for rA#1 (Figure 2C and D) compared to rA#2 (Figure 2G and H) differ at the position between N1 and the phosphate of its base pair. Given that rA_2 is the repeating unit throughout the helix and entire crystal, this alternating pattern of electron density extends along each strand of the helix (Figure 1B). For rA#1, the electron density profile is skewed, i.e. spreads from a position expected for N1 coordination to the non-bridging oxygen of its paired rA when examined at low sigma values (Figure 2D). This merged electron density appears similar to density that we have modeled as water coordinated to the 2′ OH group of the rA#2 ribose (Figure 2H). In contrast, the electron density between rA#2 N1 and the phosphate of its base pair is well-ordered, spherical with a B-factor of 18.54, and does not overlap with the non-bridging oxygen. We modeled this electron density as a coordinated ammonium ion (Figure 2E–H), as did Safaee *et al.* (9). Thus, our model illustrates water coordinated to protonated N1 of rA#1 pairs (Figure 2A–D) and ammonium coordinated to neutral adenines at rA#2 pairs (Figure 2E–H). In addition to being consistent with differences in electron densities around rA#1 and rA#2, the modeled water for rA#1 can hydrogen bond to either or both of the protonated N1 and the non-bridging phosphate oxygen to stabilize the helix. In contrast, modeling an ammonium ion at that position would be energetically unfavorable due to repulsion with the proton at N1.

Notably, adjacent helices in the crystal lattice contact one another more at each rA#2 than at each rA#1 (Figure 3). Furthermore, ammonium bound to rA#2 makes a third hydrogen bond to a non-bridging oxygen of the phosphate backbone of an adjacent helix (Figure 3). These two interactions likely lower *B*-factor values for rA#2 atoms vs. rA#1 atoms and stabilize the bundle of helices that constitute the crystal lattice, explaining why ammonium cannot be omitted from our crystallization conditions. Inversely, since rA#1 is free from making crystal contacts to the degree that typifies rA#2, the N1 protonation we observe for adenine at rA#1 might reflect a more solution-like state for rA#1 relative to rA#2 (Figure 3). The spread of electron density at rA#1 observed for the water molecule is consistent with alternative states whereby water coordinates with protonated N1 and/or its paired phosphate.

Explaining alternating protonation of N1 at each base pair and physical properties of the helix and crystal

Our rA_7 crystal structure reflects properties of the helix that rA_7 forms in acidic solution. For example, the width of our rA_7 helix is 14.9 Å from one 2′ OH to the other 2′ OH within each base pair. This width is close to the ∼12 Å-median diameter measurement obtained using atomic force microscopy for poly(rA) duplexes formed in acidic conditions and distinct from the ∼6 Å-median diameter measurement for poly(rA) at pH 8.0, which exists as a single strand (31).

In 1961, Rich *et al.* (8) predicted, based on poly(rA) fiber diffraction patterns, that the poly(rA) duplex structure has inherent 8-fold symmetry that crystallographically could be described with an asymmetric (i.e. repeating) unit of two sequential rAs having 4-fold symmetry (i.e. has a $P4_2$ space group) and a unit-cell *c*-axis of 15.2 Å, which reflects one half the pitch width of the helix. Our structure reported here in the $P4_22_12$ space group with a 14.95 Å *c*-axis con-

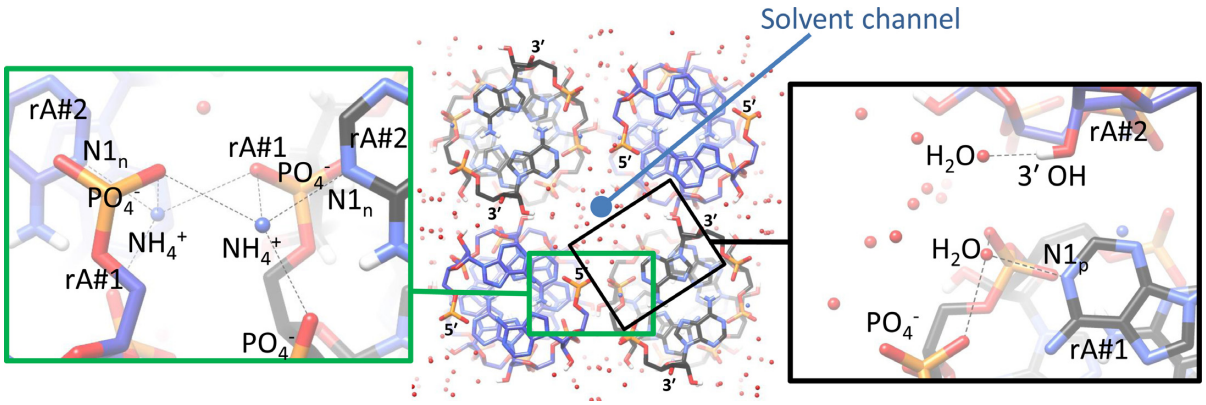

Figure 3. Ammonium ions (NH_4^+) coordinated to rA#2–rA#2 bridge inter-helical interactions within the crystal lattice. (Center) Cross-sectional view of the crystal lattice illustrating, as does Figure 1C, the alternating polarity of neighboring helices in the crystal lattice. 3'-end facing helices are denoted with black carbon atoms, and 5'-end facing helices with blue carbon atoms. Boxed insets are expanded in left and right panels. (Left) Ammonium, which is coordinated to neutral N1 (i.e. $N1_n$) of rA#2 base pairs, coordinates a non-bridging oxygen of rA#1 within the same helix and also a non-bridging oxygen of rA#1 from the adjacent helix. (Right) Water, which is coordinated to protonated N1 (i.e. $N1_p$) of rA#1 base pairs, is positioned near the open solvent channel shown in the cross-sectional view (center) and does not make appreciable inter-helical interaction as does ammonium coordinated to $N1_n$ (left).

firms this prediction. However, differences between rA#1 and rA#2 due to the presence of ammonium at every other base pair as well as the different crystal packing interactions at every other base pair are unexpected.

SUMMARY

Our X-ray crystal structure of a rA_7-generated parallel and continuous duplex in acidic conditions provides the first adenine bond angles that support the existence of N1 protonation in a parallel strand duplex of rA−rA. Our structure represents a hybrid of the X-ray fiber diffraction-derived model made by Rich *et al.* at acidic pH (8) and the ammonium-coordinated structure generated by Safaee *et al.* at neutral pH (9). Our structure reveals the remarkable ability of rA_7 to form a perfectly straight and continual helix via hybridization of overlapping strands in different registers. rA_7 crystals form in one day under inexpensive and easily reproducible conditions, possibly making them or a soluble form of them a useful nanomaterial, e.g. for sensing pH. From a material science perspective, poly(rA) duplexes could be used as a pH-sensitive switch that, when fused to other molecules, could impart a quantifiable structural change. This has also been proposed for oligo(deoxy-rA), which has likewise been reported to duplex at lower pH (32). However, there is no available structure for oligo(deoxy-rA).

The structures presented here and by Safaee et al. (9) may provide important insights into other recent studies that involve poly(rA) structures. For example, a study of thioflavin T, a fluor that interacts with purine-containing nucleic acids in a way that is not completely understood, was found to less effectively label heat-denatured rA_{50} compared to heat-denatured deoxy-rA_{50}, suggesting secondary structure differences such as poly(rA) duplex formation (33). Furthermore, melting and circular dichroism studies revealed that poly(rA) duplexes form at neutral pH on single-walled carbon nanotubes when the nanotubes are modified with either COOH or CH_2OH (34).

Of course, a critical issue that remains to be resolved is whether poly(rA) duplexes form in living cells. Important to living organisms, most transcripts synthesized by RNA polymerase II have a 3' end of poly(rA) (35). While the cell does not normally contain substantial concentrations of ammonium ions and is generally not acidic, protein mediation, acidic cellular compartments, metabolic conditions, or environmental acidic stress could possibly induce duplexed poly(rA) to form in living cells. As has been hypothesized (36), the formation of duplexed poly(rA) during the nuclear process of polyadenylation could limit poly(rA) lengthening, thereby regulating mRNA 3' poly(rA) size, or increase mRNA half-life in the cytoplasm by protecting mRNAs from 3'-to-5' deadenylases that degrade single-stranded poly(rA). The structure reported here may facilitate design of reagents able to detect parallel stranded poly(rA) helices in cells and elsewhere.

SUPPLEMENTARY DATA

Supplementary Data are available at NAR Online.

ACKNOWLEDGEMENTS

The authors thank J.J. Jenkins for X-ray data collection and related support; C. Kielkopf and J. Wedekind for sharing cryocrystallography and shipping tools; K. Gehring, G. Sheldrick, G. Thurston and J. Wedekind for helpful discussions, and the referees for very thoughtful and helpful comments. We also thank A. Gonzalez and Y. Tsai at the Stanford Synchrotron Radiation Lightsource (SSRL) for the autoXDS program.

FUNDING

Research was supported by the National Institutes of Health (NIH) National Institute of General Medical Sciences [R37 GM074593 to L.E.M., R01 GM22939 to D.H.T.], and the National Cancer Institute [T32 CA09363, which supported M.L.G. for part of the time]. The University of Rochester Medical Center Structural Biology

and Biophysics Facility is supported by the NIH National Center for Research Resources [1S10 RR026501, 1S10 RR027241], the NIH National Institute of Allergy and Infectious Diseases [P30 AI078498], and the University of Rochester School of Medicine and Dentistry. The SSRL Structural Molecular Biology Program is supported by the Department of Energy Office of Biological and Environmental Research, the NIH National Center for Research Resources Biomedical Technology Program [P41RR001209], and the NIH National Institute of General Medical Sciences. Funding for open access charge: NIH [R37 GM074593 to L.E.M.].
Conflict of interest statement. None declared.

REFERENCES

1. Lee,H., Lytton-Jean,A.K., Chen,Y., Love,K.T., Park,A.I., Karagiannis,E.D., Sehgal,A., Querbes,W., Zurenko,C.S., Jayaraman,M. *et al.* Molecularly self-assembled nucleic acid nanoparticles for targeted in vivo siRNA delivery. *Nat. Nanotechnol.*, **7**, 389–393.
2. Musumeci,D., Riccardi,C. and Montesarchio,D. (2015) G-quadruplex forming oligonucleotides as anti-HIV agents. *Molecules*, **20**, 17511–17532.
3. Sun,W. and Gu,Z. (2015) Engineering DNA scaffolds for delivery of anticancer therapeutics. *Biomater. Sci.*, **3**, 1018–1024.
4. Fresco,J.R. and Doty,P. (1957) Polynucleotides. I. Molecular properties and configurations of polyriboadenylic acid in solution. *J. Am. Chem. Soc.*, **79**, 3928–3929.
5. Fresco,J.R. and Klemperer,E. (1959) Polyriboadenylic acid, a molecular analogue of ribonucleic acid and desoxyribonucleic acid. *Ann. N. Y. Acad. Sci.*, **81**, 730–741.
6. Applequist,J. and Damle,V. (1965) Thermodynamics of helix-coil equilibrium in oligoadenylic acid from hypochromicity studies. *J. Am. Chem. Soc.*, **87**, 1450–1458.
7. Brahms,J., Michelson,A.M. and Van Holde,K.E. (1966) Adenylate oligomers in single- and double-strand conformation. *J. Mol. Biol.*, **15**, 467–488.
8. Rich,A., Davies,D.R., Crick,F.H. and Watson,J.D. (1961) The molecular structure of polyadenylic acid. *J. Mol. Biol.*, **3**, 71–86.
9. Safaee,N., Noronha,A.M., Rodionov,D., Kozlov,G., Wilds,C.J., Sheldrick,G.M. and Gehring,K. (2013) Structure of the parallel duplex of poly(A) RNA: evaluation of a 50 year-old prediction. *Angew. Chem. Int. Ed. Engl.*, **52**, 10370–10373.
10. Halder,A., Halder,S., Bhattacharyya,D. and Mitra,A. (2014) Feasibility of occurrence of different types of protonated base pairs in RNA: a quantum chemical study. *Phys. Chem. Chem. Phys.*, **16**, 18383–18396.
11. Kapinos,L.E., Operschall,B.P., Larsen,E. and Sigel,H. (2011) Understanding the acid-base properties of adenosine: the intrinsic basicities of N1, N3 and N7. *Chemistry*, **17**, 8156–8164.
12. Markowski,V., Sullivan,G.R. and Roberts,J.D. (1977) Nitrogen-15 nuclear magnetic resonance spectroscopy of some nucleosides and nucleotides. *J. Am. Chem. Soc.*, **99**, 714–718.
13. Touboul,D., Bouchoux,G. and Zenobi,R. (2008) Gas-phase protonation thermochemistry of adenosine. *J. Phys. Chem. B*, **112**, 11716–11725.
14. Green-Church,K.B. and Limbach,P.A. (2000) Mononucleotide gas-phase proton affinities as determined by the kinetic method. *J. Am. Soc . Mass Spectrom.*, **11**, 24–32.
15. Russo,N., Toscano,M., Grand,A. and Jolibois,F. (1998) Protonation of thymine, cytosine, adenine, and guanine DNA nucleic acid bases: Theoretical investigation into the framework of density functional theory. *J. Computat. Chem.*, **19**, 989–1000.
16. Xia,F., Xie,H. and Cao,Z. (2008) Density functional study of protonation of deoxynucleosides: Electrophilic active sites and proton affinities. *Int. J. Quant. Chem.*, **108**, 57–65.
17. Evans,P. (2006) Scaling and assessment of data quality. *Acta Crystallogr. D Biol. Crystallogr.*, **62**, 72–82.
18. Kabsch,W. (2010) Xds. *Acta Crystallogr. D Biol. Crystallogr.*, **66**, 125–132.
19. McCoy,A.J., Grosse-Kunstleve,R.W., Adams,P.D., Winn,M.D., Storoni,L.C. and Read,R.J. (2007) Phaser crystallographic software. *J. Appl. Crystallogr.*, **40**, 658–674.
20. Adams,P.D., Afonine,P.V., Bunkoczi,G., Chen,V.B., Davis,I.W., Echols,N., Headd,J.J., Hung,L.W., Kapral,G.J., Grosse-Kunstleve,R.W. *et al.* (2010) PHENIX: a comprehensive Python-based system for macromolecular structure solution. *Acta Crystallogr. D Biol. Crystallogr.*, **66**, 213–221.
21. Emsley,P., Lohkamp,B., Scott,W.G. and Cowtan,K. (2010) Features and development of Coot. *Acta Crystallogr. D Biol. Crystallogr.*, **66**, 486–501.
22. Winn,M.D., Ballard,C.C., Cowtan,K.D., Dodson,E.J., Emsley,P., Evans,P.R., Keegan,R.M., Krissinel,E.B., Leslie,A.G., McCoy,A. *et al.* (2011) Overview of the CCP4 suite and current developments. *Acta Crystallogr. D Biol. Crystallogr.*, **67**, 235–242.
23. Becke,A.D. (1993) Density-functional thermochemistry. III. The role of exact exchange. *J. Chem. Phys.*, **98**, 5648–5652.
24. Lee,C., Yang,W. and Parr,R.G. (1988) Development of the Colle-Salvetti correlation-energy formula into a functional of the electron density. *Phys. Rev. B Condens. Matter*, **37**, 785–789.
25. Dror,O., Nussinov,R. and Wolfson,H.J. (2006) The ARTS web server for aligning RNA tertiary structures. *Nucleic Acids Res.*, **34**, W412–W415.
26. Lu,X.J. and Olson,W.K. (2003) 3DNA: a software package for the analysis, rebuilding and visualization of three-dimensional nucleic acid structures. *Nucleic Acids Res.*, **31**, 5108–5121.
27. Colasanti,A.V., Lu,X.J. and Olson,W.K. Analyzing and building nucleic acid structures with 3DNA. *J. Vis. Exp.*, e4401.
28. Meents,A., Dittrich,B. and Gutmann,S. (2009) A new aspect of specific radiation damage: hydrogen abstraction from organic molecules. *J. Synchrotron Radiat.*, **16**, 183–190.
29. Petrova,T. and Podjarny,A. (2004) Protein crystallography at subatomic resolution. *Rep. Progr. Phys.*, **67**, 1565–1605.
30. Taylor,R. and Kennard,O. (1982) The molecular structure of nucleosides and nucleotides: Part 1. The influence of protonation on the geometries of nucleic acid constituents. *J. Mol. Struct.*, **78**, 1–28.
31. Ke,C., Loksztejn,A., Jiang,Y., Kim,M., Humeniuk,M., Rabbi,M. and Marszalek,P.E. (2009) Detecting solvent-driven transitions of poly(A) to double-stranded conformations by atomic force microscopy. *Biophys. J.*, **96**, 2918–2925.
32. Chakraborty,S., Sharma,S., Maiti,P.K. and Krishnan,Y. (2009) The poly dA helix: a new structural motif for high performance DNA-based molecular switches. *Nucleic Acids Res.*, **37**, 2810–2817.
33. Sugimoto,S., Arita-Morioka,K., Mizunoe,Y., Yamanaka,K. and Ogura,T. (2015) Thioflavin T as a fluorescence probe for monitoring RNA metabolism at molecular and cellular levels. *Nucleic Acids Res.*, **43**, e92.
34. Zhao,C., Peng,Y., Song,Y., Ren,J. and Qu,X. (2008) Self-assembly of single-stranded RNA on carbon nanotube: polyadenylic acid to form a duplex structure. *Small*, **4**, 656–661.
35. Proudfoot,N.J. (2011) Ending the message: poly(A) signals then and now. *Genes Dev.*, **25**, 1770–1782.
36. Zarudnaya,M.I. and Hovorun,D.M. (1999) Hypothetical double-helical poly(A) formation in a cell and its possible biological significance. *IUBMB Life*, **48**, 581–584.